Double Lorentzian atomic prism

David J. Starling, Steven M. Bloch, Praveen K. Vudyasetu, Joseph S. Choi, Bethany Little, and John C. Howell

A double resonance atomic prism

David J. Starling,[1] Steven M. Bloch,[1] Praveen K. Vudyasetu,[1] Joseph S. Choi,[1,2] Bethany Little,[1] and John C. Howell[1]

[1] *Department of Physics and Astronomy, University of Rochester, Rochester, NY 14627, USA*
[2] *The Institute of Optics, University of Rochester, Rochester, NY 14627, USA*

We present an atomic prism spectrometer that utilizes the steep linear dispersion between two strongly absorbing hyperfine resonances of rubidium. We resolve spectral lines 50 MHz apart and, utilizing a larger part of the available spectrum than only between the two resonances, we spatially separate collinear pump, signal and idler beams resulting from a four-wave mixing process. Due to the high transparency possible between the resonances, these results have applications in the filtering of narrow band entangled photons and interaction free measurements.

I. INTRODUCTION

Devices exhibiting high spectral resolution are invaluable in the field of photonics. Common techniques for high resolution spectroscopy use Fourier transform interferometers [1], Fabry-Perot cavities [2–4], optical frequency combs [4–6] and Faraday rotation with polarization optics [7–9]. Here, we present an atomic prism spectrometer which utilizes the steep linear dispersion between two strongly absorbing rubidium (Rb) resonances to achieve high spectral resolution. We demonstrate the sensitivity of the prism by discriminating spectral lines 50 MHz apart with 36% transmission, and 190 MHz apart with 80% transmission. We also spatially separate collinear pump, signal and idler beams resulting from a four-wave mixing (FWM) process [10] and show up to 35 dB suppression over a 1.4 GHz bandwidth. These results highlight the potential for use in interaction free measurements [9], the filtering of entangled photons [11] or frequency modes from atomic interactions, the separation of multiple teeth of an optical frequency comb [12–14], and even the filtering of (frequency) multimode images [15].

The large dispersion near an atomic resonance is well known [16, 17], and its use in spectroscopy has been studied extensively in metal vapors [18–24]. Early experiments have focused on a single absorption [19, 20, 25] or transmission [18] resonance. For example, Finkelstein *et al.* showed that, using the resonance enhancement of dispersion of a single absorption line, a mercury vapor prism could resolve the Raman lines of CO_2 [20]. Related work in the area of interaction-free measurement has shown filtering of an 80 MHz line with 35 dB suppression near an atomic resonance [9]. However, the utility of this system is diminished by the low (10%) transmission. It is therefore advantageous to consider using the transparent region between two resonances where there is increased bandwidth, decreased frequency-dependent absorption, high transparency and the ability to resolve many spectral lines.

Here, we present a Rb vapor prism spectrometer that operates in the transparent region between two strongly absorbing resonances. Such a transparent region also gives rise to slow light and has been studied in various systems recently [26]. We show that the number of resolvable spectral frequencies between the resonances—which is an important feature of this design—is proportional to the slow light delay-bandwidth product. The delay-bandwidth product for double absorption slow light has been shown to be nearly 50 in Rb [27] and 100 in cesium [28]; therefore, there may exist advantages over electromagnetically induced transparency (EIT) [10] based slow light prisms [18], where the delay-bandwidth products are typically less than one. In addition, the separation of frequency modes is independent of polarization, in contrast to EIT [18] and Faraday anomalous dispersion optical filters [7–9].

In section II, we derive the dispersion and the minimum resolvable frequency separation for an atomic prism operating in the transparent region between two resonances. We include a discussion of an overall shift in the position due to absorption in the prism. In section III, we describe the experiment and find a trade-off between bandwidth and dispersion. We therefore utilize two different prisms: one with more bandwidth, and one with more dispersion. Section III is followed by a discussion of the results and a conclusion.

II. THEORY

Consider a double absorption slow light medium [27] of Rb vapor in an evacuated chamber. The chamber is placed in air as shown in Fig. 1a and the shape of the chamber is a prism with an apex angle of θ_0. Assuming that the index of refraction of air is unity, the change in the direction of the beam at the exit interface is small. We can obtain the exit angle of the ray after propagating through the prism as $n(\nu)\sin(\theta_0) = \sin[\theta(\nu)]$, where $n(\nu)$ is the real part of the index of refraction and $\theta(\nu)$ is the angle made by the ray with the normal of the second surface of the prism as shown in Fig. 1b. For $n(\nu) \approx 1$, the angular dispersion of frequencies can be written as

$$\frac{d\theta}{d\nu} \approx A\frac{dn}{d\nu}, \qquad (1)$$

where we assumed small deflections and A is a geometric factor determined by θ_0 and the incidence angle. The values of A will be given in the experimental section.

The quantity $dn/d\nu$ depends on the system of interest. However, we know that the group index $n_g =$
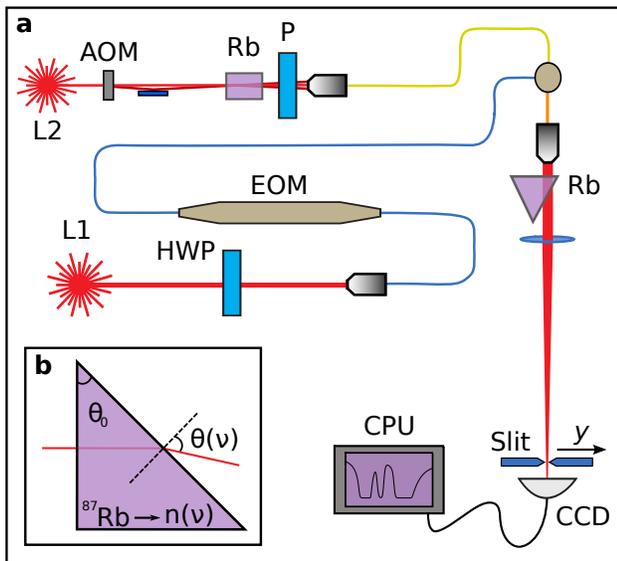
FIG. 1. (color online) The experimental setup. (a) Laser L2 is frequency modulated by an acousto-optic modulator (AOM), generating two coherent beams separated by 3.035 GHz. These beams interact via FWM in a hot Rb vapor cell, producing signal and idler beams which pass through a polarizer (P) and into a single mode fiber (yellow). The pump beam is vertically polarized and the signal and idler beams are horizontally polarized. Alternatively, laser L1 is coupled into a fiber electro-optic modulator (EOM, blue). We pass the output from either fiber through a prism filled with Rb and then focus the beam onto a CCD camera. A variable width slit can be inserted into the path, at the focus of the beam. (b) A detailed diagram of the geometry of the prism. The real part of the index of refraction of the prism $n(\nu)$ and the output angle of the beam $\theta(\nu)$ depend on the laser frequency ν.

$n + \nu dn/d\nu \approx \nu dn/d\nu$, for large dispersion. Therefore, we can replace $dn/d\nu$ with n_g/ν. For a medium of length L and a group delay of τ, $n_g/\nu \approx \lambda\tau/L$ where λ is the wavelength and we assumed that $n_g \gg 1$ [27]. The group delay in a double absorption system is approximately given by $\tau = \alpha L/\Gamma$, where α is the absorption coefficient at the center of the transparency and Γ is the full width at half maximum of each absorption [27]. The resulting angular dispersion is therefore given by

$$\frac{d\theta}{d\nu} = A\frac{\lambda\alpha}{\Gamma}. \tag{2}$$

We are particularly interested in the number of spatially resolvable frequency modes. However, for small frequency changes $\Delta\nu$, $\Delta\theta$ is typically not sufficient to spatially separate each mode. We therefore place a lens of focal length f near the exit face of the prism (or, right before the prism); this results in a displacement of the beam of $\Delta y = \Delta\theta(\nu)f$ in the focal plane. For a beam with a $(1/e^2)$ Gaussian diameter of D before the lens, the Fourier transform limited diameter of the beam at the focal plane is given by $d = \frac{4\lambda}{\pi}\frac{f}{D}$. We then place a

detector in this plane and calculate the amount of frequency shift needed for one beam waist displacement of the beam. Setting $\Delta y = d$, we find

$$\Delta\nu_{\min} = \frac{d}{fA}\frac{L}{\lambda\tau} = \frac{4\Gamma}{A\pi\alpha D}. \tag{3}$$

This quantity gives us the minimum frequency resolution of the prism. We note that f/d is linearly related to D, the Gaussian beam diameter before the lens. Therefore, $\Delta\nu_{\min}$ is independent of the focal length of the lens.

Similarly, to spatially separate *multiple* frequency components, we require $\Delta y_{\max}/d \gg 1$, where $\Delta y_{\max}$ is the maximum deflection for the system. That is, we want

$$\frac{\Delta y_{\max}}{d} = \frac{f\lambda A}{d}\frac{\tau\Delta\nu_{\max}}{L} \gg 1, \tag{4}$$

where $\Delta\nu_{\max}$ is the bandwidth of the prism. We see that this ratio is proportional to the delay-bandwidth product over unit length.

In order to maximize $\Delta y_{\max}/d$ we need a slow light system with a large delay-bandwidth product, such as a double Lorentzian absorption system. The bandwidth of the system is governed by the separation between the two absorptions and the delay is dependent on the optical depth. The hyperfine absorption lines in alkali metals (e.g., Rb or Cs) provide ideal double absorption resonances for this purpose.

The simplified model discussed above can predict our experimental results. However, for more accuracy, we need to consider the effect of a centroid shift due to differential absorption across the transverse cross-section of the beam in the prism. Since there is a uniform extinction coefficient in the prism, the part of the beam with the longest path length within the prism will have the largest amount of loss. The intensity of the beam after propagating through the prism is given by $I = I_0 \exp[-2(x - x_0)^2/w^2]\exp(-\alpha L_0 x/x_0)$ where I_0 is the intensity at the center of the beam before the prism, α is the absorption coefficient, L_0 is the propagation distance for the centroid when there is no absorption, w is the Gaussian beam radius $(D/2)$ and x_0 is the distance of the beam from the vertex of the prism. The intensity I can be rewritten as $I = I'\exp\{-2\left[x - (x_0 - \alpha L_0 w^2/4x_0)\right]^2/w^2\}$ where $I' = I_0\exp(-\alpha L_0)\exp(\alpha^2 w^2 L_0^2/8x_0^2)$. The centroid of the Gaussian beam is thus shifted by $\alpha L_0 w^2/4x_0$. For the experimental results below, this shift is approximately 2-4% of the width of the beam. We note that L and τ in all the equations correspond to the length of propagation and delay for the *centroid* of the exit beam.

III. EXPERIMENT

The schematic of the experimental setup is shown in Fig. 1. We analyze two sources: the frequency sidebands generated by laser L1 passing through an EOM and the FWM signal generated by the nonlinear interaction of
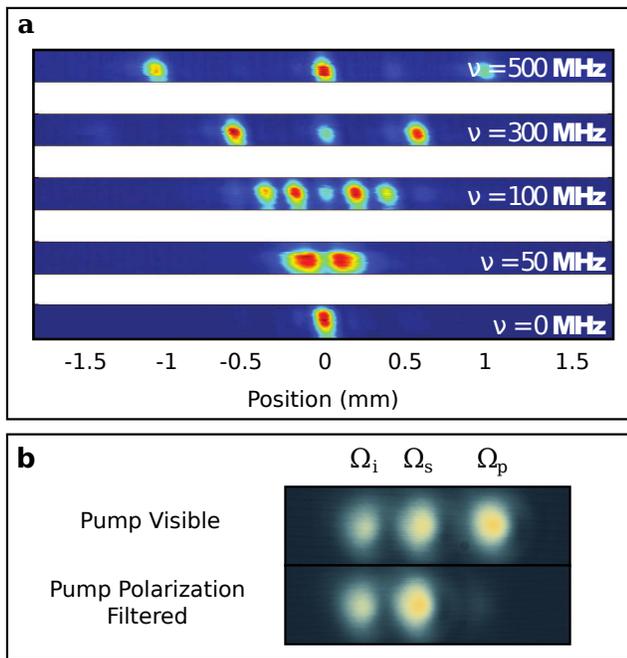
FIG. 2. (color online) Camera data. (a) The transverse profile of the beam at the detector for different modulation frequencies ν using the naturally abundant Rb prism. The central lobe corresponds to the zeroth order frequency and the other lobes correspond to sidebands. (b) We spatially discriminate the different modes generated from FWM using the isotopically pure ^{87}Rb prism. Ω_j is the Rabi frequency of the jth mode (signal, idler and pump).

laser L2 with atomic Rb. As we change the frequency of the source between the atomic resonances, we see a shift in the position of the beam at the camera. We note that the displacement of the beam as well as its focal spot size increase for longer focal distance. We consider two atomic prisms to emphasize different aspects of this design. The first prism contains naturally abundant Rb, resulting in steep dispersion at the cost of bandwidth. The second prism contains isotopically pure ^{87}Rb, offering a larger transparent region. Below, we describe the details of each frequency source and each prism.

Frequency source 1 — A narrow line width external cavity diode laser at 780 nm was tuned near the hyperfine resonances of the D_2 line of Rb and coupled into a fiber EOM which was driven by an oscillator. A $\lambda/2$ wave plate was used to control the efficiency of the sideband creation. We vary the frequency modulation of the EOM from DC to 550 MHz.

Frequency source 2 — A narrow line width external cavity diode laser was frequency shifted with a 1.5 GHz acousto-optic modulator, double passed, to produce two linearly but orthogonally polarized coherent beams separated by 3.035 GHz. This separation corresponds to the ground state hyperfine splitting of ^{85}Rb. These beams were combined at a polarizing beam splitter and passed through a magnetically shielded, heated vapor cell

with naturally abundant Rb and 20 Torr neon buffer gas. The frequencies and powers of each beam were adjusted to produce collinear FWM within the vapor cell. In particular, the signal beam was tuned to the blue of the $F = 3 \rightarrow F' = \{2, 3\}$ ^{85}Rb transition and the pump beam, separated by 3.035 GHz in frequency from the signal beam, was therefore to the blue of the $F = 2 \rightarrow F' = \{2, 3\}$ ^{85}Rb transition. An idler beam is generated, 3.035 GHz in frequency to the blue of the pump beam. The output was polarization filtered to remove the pump and coupled into a single mode fiber.

The light from each source was then separately passed through a hot Rb vapor prism and either focused onto an 8-bit CCD camera or a slit in the focal plane with a power meter. The intensity profile was then observed for each source. We considered two different prisms to emphasize 1) high dispersion or 2) large bandwidth.

Prism 1 (naturally abundant Rb) — The ground state hyperfine splitting of ^{85}Rb and ^{87}Rb is 3.035 GHz and 6.835 GHz respectively, and the relative populations are 72.2% and 27.8% respectively. The prism had a 79° apex angle and the beam was 20° from perpendicular incidence, giving a geometric factor $A \approx 2$. The beam was focused gently through the prism and on to a camera; the cell was 3 cm from the lens, which was 38 cm from the camera. The Gaussian diameter of the beam before the cell was $D = 1.6$ mm and the centroid propagated about 6 mm through the prism. The focused Gaussian diameter d at the camera was approximately 90 μm.

Prism 2 (isotopically pure ^{87}Rb) — The prism contained approximately 98% ^{87}Rb (2% ^{85}Rb) and was heated to approximately 114°C. It had a 45° apex angle. The light entered the vapor cell perpendicular to the face of the Rb prism and exited through the other side as shown in Fig. 1b, resulting in a geometric factor of $A \approx 1$. The beam had a Gaussian diameter of $D = 3.8$ mm and the centroid propagated about 3.1 mm through the prism. The beam was focused on the camera 1 m away. The focused Gaussian diameter d at the camera was approximately 260 μm.

Even though the dispersion increases for higher temperatures of the vapor cell, the effective bandwidth of the system decreases due to increased absorption. At our working temperature, the bandwidth of our system was about 1.1 GHz with 36% transmission for the naturally abundant prism, and 1.8 GHz with 80% transmission for the isotopically pure ^{87}Rb prism. Note that, for each prism, we report data only in the largest transparency window; however, there are other, narrower regions for each prism which result in larger dispersion.

IV. RESULTS

Let us first consider the source from laser L1 using the naturally abundant prism. The frequency dependent deflection is quantified by first turning off the EOM and tuning the frequency of L1 to the center of the trans-

parency between the two ^{85}Rb resonances. Turning on the EOM results in frequency sidebands. Different frequency bands in the signal are spatially separated after the prism and the resultant spatial distribution of intensities is recorded at the camera. Fig. 2a shows the data for different modulation frequencies. The central spot is the zeroth order (unmodulated) frequency followed by the first order and second order sidebands to either side. The first order sidebands are visible up to the modulation frequency of 550 MHz. Frequency dependent absorption causes the change in relative intensities of each mode; one can obtain the exact spectral information of the input signal by correcting for the frequency dependent losses at the vapor cell. The transmission of the zeroth order beam through the prism is approximately 36%. With a bandwidth of 1.1 GHz, we find that the displacement at the camera is 1.95 ± 0.10 μm/MHz. With a 0.38 m focal length lens, this corresponds to an angular dispersion of 5.1 ± 0.3 μrad/MHz, and so $dn/d\nu \approx (2.6 \pm 0.1) \times 10^{-12}$ Hz^{-1}. Based upon simulations including the entire spectrum of naturally abundant rubidium with Doppler broadening, we expect the dispersion to be approximately $dn/d\nu \approx 3.5 \times 10^{-12}$ Hz^{-1}. This is in fair agreement with the experimental result. Note that, for a glass prism, $dn/d\nu$ is five orders of magnitude less, at 4×10^{-17} Hz^{-1}.

We also find that our figures of merit are $\Delta y_{\max} = 2.15$ mm and $\Delta\nu_{\min} = 50$ MHz. Using Eq. (4), for a delay of 26 ns and propagation length of 6 ± 1 mm, we expect a maximum deviation of 2.6 ± 0.4 mm. From Eq. (3), using the measured focal spot size, we expect a spatial frequency resolution $\Delta\nu_{\min}$ of 37 ± 6 MHz. The error bars are the result of the uncertainty of the propagation length L. These predictions are in fair agreement with our experimental results; the largest contribution to the error is likely due to the deviation of the dispersion from our simplified model as well defects in the optical elements.

We now consider the source from laser L2 using the isotopically pure ^{87}Rb prism. By using the transparent region between the ^{87}Rb resonances as well as the much larger nonlinear dispersive region outside the resonances, we spatially separate different frequencies resulting from a collinear FWM process in ^{85}Rb. The setup is similar to the FWM discussed in ref. 29. Signal, idler and pump beams at the output of a Rb vapor cell are coupled into a fiber (yellow in Fig. 1a). Signal and pump beams fall in the highly dispersive region between the resonances. The magnitude of the deflection is different for each mode due to the different refractive indicies of Rb at their respective frequencies. The idler beam, which is about 6 GHz to the blue of signal beam, is farther from resonance and hence experiences less deflection. Fig. 2b shows the image at the detector. The central spot is the signal beam and the left and right spots are of idler and pump, respectively. The transmission of the signal photons is 80%, falling in the transparent region of the prism. We see that each mode is well separated with low loss.
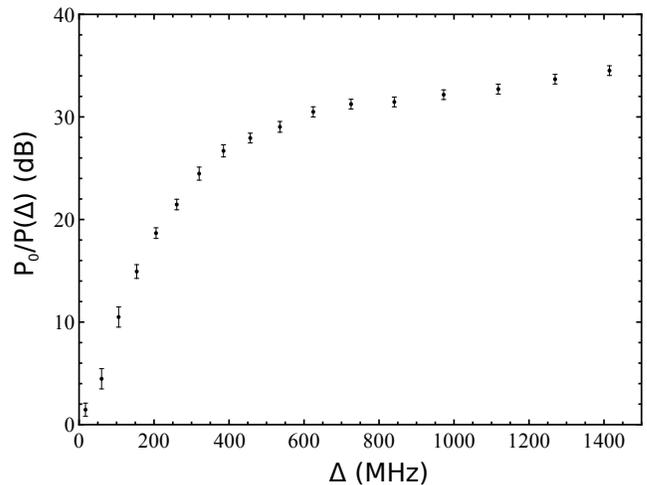
FIG. 3. Extinction ratio. The suppression of one frequency mode relative to another, separated by Δ, using the isotopically pure ^{87}Rb prism. See text for details.

While transparency is a key feature of this design, many entanglement applications require high relative suppression as well to filter background and reduce crosstalk. We therefore compare the amount of light that passes through a slit positioned in the focal plane at different frequency modes. The slit is roughly 200 μm in width to match the size of the beam in the focal plane. A single frequency ν is passed through the prism. P_0 is defined as the power, *measured through the slit*, of frequency mode ν. Approximately 70% of the incident light (28 μW) passes through the slit at this slit location. $P(\Delta)$ is then defined as the power, measured through the slit, of frequency mode $\nu + \Delta$. Note that the frequency source remains fixed at frequency ν and is set to the blue edge of the large transparency region of the isotopically pure ^{87}Rb prism. Using this highly transparent prism, we find that beams separated by 600 MHz have greater than 30 dB relative suppression, with a max of about 35 dB across the transparent region of 1.4 GHz, as shown in Fig. 3. The experimentally determined suppression plateaus at large frequency separations, in contrast to theoretical predictions, due to scattered light from the prism. The errors bars are estimates of the maximum random error of the power measurements at each slit location. We find that modes approximately $\Delta\nu_{\min} = 190$ MHz apart are well separated.

V. CONCLUSION

In summary, we have demonstrated a highly dispersive atomic prism. We showed that the number of resolvable spectral frequencies is proportional to the delay-bandwidth product, which makes a slow light double absorption system an attractive choice for an atomic prism. These ideas can be generalized to larger bandwidth sys-

tems; for example, one can utilize linear dispersion between the D_1 and D_2 absorption frequencies of Rb [30]. Furthermore, we demonstrated a spatial separation of the pump, signal and idler beams from a FWM process in Rb and find a suppression of 35 dB between frequencies separated by 1.4 GHz with 80% transmission.

[1] Z. Shi, R. W. Boyd, R. M. Camacho, P. K. Vudyasetu, and J. C. Howell, Phys. Rev. Lett. **99**, 240801 (2007).

[2] P. Hariharan, *Optical interferometry* (Elsevier Science, Amsterdam, 2003).

[3] S. Saraf, R. L. Byer, and P. J. King, Appl. Opt. **46**, 3850 (2007).

[4] M. J. Thorpe, D. Balslev-Clausen, M. S. Kirchner, and J. Ye, Opt. Express **16**, 2387 (2008).

[5] R. H. T. Udem and T. W. Hänsch, Nature **416**, 233 (2002).

[6] A. Foltynowicz, P. Maslowski, T. Ban, F. Adler, K. C. Cossel, T. C. Briles, and J. Ye, Faraday Discuss. **150**, (2011).

[7] R. P. Abel, U. Krohn, P. Siddons, I. G. Hughes, and C. S. Adams, Opt. Lett. **34**, 3071 (2009).

[8] J. A. Zielińska, F. A. Beduini, N. Godbout, and M. W. Mitchell, Opt. Lett. **37**, 524 (2012).

[9] F. Wolfgramm, Y. A. de Icaza Astiz, F. A. Beduini, A. Cerè, and M. W. Mitchell, Phys. Rev. Lett. **106**, 053602 (2011).

[10] M. Fleischhauer, A. Imamoglu, and J. P. Marangos, Rev. Mod. Phys. **77**, 633 (2005).

[11] R. Okamoto, J. L. O'Brien, H. F. Hofmann, T. Nagata, K. Sasaki, and S. Takeuchi, Science **323**, 483 (2009).

[12] M. C. Stowe, M. J. Thorpe, A. Pe'er, J. Ye, J. E. Stalnaker, V. Gerginov, and S. A. Diddams (Academic Press, 2008) pp. 1 – 60.

[13] S. A. Diddams, L. Hollberg, and V. Mbele, Nature **445**, 627 (2007).

[14] A. Bartels, D. Heinecke, and S. A. Diddams, Science **326**, 681 (2009).

[15] P. K. Vudyasetu, R. M. Camacho, and J. C. Howell, Phys. Rev. Lett. **100**, 123903 (2008).

[16] R. W. Wood, *Physical Optics* (Optical Society of America, 1988).

[17] W. C. Marlow, Appl. Opt. **6**, 1715 (1967).

[18] V. A. Sautenkov, H. Li, Y. V. Rostovtsev, and M. O. Scully, Phys. Rev. A **81**, 063824 (2010).

[19] A. Zheltikov, A. Naumov, P. Barker, and R. Miles, Optics and Spectroscopy **89**, 282 (2000), 10.1134/1.1307448.

[20] N. D. Finkelstein, A. P. Yalin, W. R. Lempert, and R. B. Miles, Opt. Lett. **23**, 1615 (1998).

[21] N. D. Finkelstein, W. R. Lempert, and R. B. Miles, Opt. Lett. **22**, 537 (1997).

[22] A. P. Yalin, P. F. Barker, and R. B. Miles, Opt. Lett. **25**, 502 (2000).

[23] D. Hoffman, K.-U. Münch, and A. Leipertz, Opt. Lett. **21**, 525 (1996).

[24] J. Menders, K. Benson, S. H. Bloom, C. S. Liu, and E. Korevaar, Opt. Lett. **16**, 846 (1991).

[25] S.-Y. Lin, V. M. Hietala, L. Wang, and E. D. Jones, Opt. Lett. **21**, 1771 (1996).

[26] J. B. Khurgin, Adv. Opt. Photon. **2**, 287 (2010).

[27] R. M. Camacho, M. V. Pack, and J. C. Howell, Phys. Rev. A **73**, 063812 (2006).

[28] R. M. Camacho, M. V. Pack, J. C. Howell, A. Schweinsberg, and R. W. Boyd, Phys. Rev. Lett. **98**, 153601 (2007).

[29] P. K. V. Ryan M. Camacho and J. C. Howell, Nature Photonics **3**, 103 (2009).

[30] C. J. Broadbent, R. M. Camacho, R. Xin, and J. C. Howell, Phys. Rev. Lett. **100**, 133602 (2008).